Ru-Doped Cobalt−Zirconia Nanocomposites by Flame Synthesis: Physicochemical and Catalytic Properties

Wey Yang Teoh,[†] Ridwan Setiawan,[†] Lutz Mädler,[‡] Jan-Dierk Grunwaldt,[§] Rose Amal,*[,†] and Sotiris E. Pratsinis[||]

ARC Centre of Excellence for Functional Nanomaterials, School of Chemical Sciences and Engineering, The University of New South Wales, Sydney, NSW 2052, Australia, Foundation Institute of Materials Science (IWT), Department of Production Engineering, University of Bremen, 28359 Bremen, Germany, Department of Chemical and Biochemical Engineering, Technical University of Denmark, DK-2800 Lyngby, Denmark, and Particle Technology Laboratory, Institute of Process Engineering, Department of Mechanical and Process Engineering, Swiss Federal Institute of Technology (ETH) Zürich, CH-8092 Zürich, Switzerland

Received January 26, 2008. Revised Manuscript Received March 6, 2008

Nanocomposites of Ru-doped cobalt−zirconia (20 wt % Co) were made by rapid and scalable flame spray pyrolysis (FSP). They were characterized by nitrogen adsorption, X-ray diffraction, electron microscopy, and X-ray photoelectron spectroscopy revealing that cobalt clusters were highly dispersed within the zirconia matrix. Adding traces of Ru (0.04 and 0.4 wt %) to this unique structure during FSP significantly lowered the two-step reduction temperature of Co_3O_4 to CoO and metallic Co^0, further resulting in a 4-fold increase in CO chemisorption compared to undoped ones. The catalytic properties of the nanocomposites were further studied in a Fischer−Tropsch reaction and compared to those prepared by incipient wetness impregnation and mechanical mixing. The enhanced reducibility and CO chemisorption through doping with 0.4 wt % Ru was highly beneficial to the catalytic property of the flame-made composites.

1. Introduction

Cobalt is one of the most heavily investigated transition metals for heterogeneous catalytic applications. In the form of supported single element or alloys, cobalt is an interesting material that finds presence in various reactions ranging from catalytic combustion,[1,2] steam reforming,[3,4] ammonia synthesis,[5] abatement of NO_x[6–8] and CO,[9] to Fischer−Tropsch (FT) synthesis.[10–13] In particular, the search for active FT materials to yield ultraclean long-chain paraffins (synthetic diesel) has dominated the literature body of inorganic cobalt-based materials in the past decade. Nevertheless, the materials design has largely revolved around wet chemistry techniques[14–19] and hence the structure−performance relationship of other synthesis methods has been limited.

Traditionally, cobalt is deposited onto various metal oxide supports such as alumina,[14,15] silica,[15–18] titania,[15,19] and to a much lesser extent zirconia[14,19] via the multistep and sequential approaches of incipient wetness impregnation (IWI), sol−gel, or precipitation. Cobalt supported on alumina and titania is often limited by the strong cobalt oxide−support interaction.[15] The formation of irreducible cobalt silicate by reaction of cobalt oxide and silica during reduction step has also been reported.[17] These characteristics in turn limit the catalytic performance of cobalt. On the other hand, zirconia is frequently used as a promoter to enhance the cobalt dispersion on existing supports of alumina[15,20,21] or silica.[15,22] It is thought that the mild metal−support interaction of cobalt

* Corresponding author. E-mail: r.amal@unsw.edu.au. Tel.: 61 2 9385 4361, Fax.:61 2 9385 5966.
[†] The University of New South Wales.
[‡] University of Bremen.
[§] Technical University of Denmark.
[||] Swiss Federal Institute of Technology (ETH) Zürich.

(1) Milt, V. G.; Ulla, M. A.; Lombardo, E. A. *J. Catal.* **2001**, *200*, 241.
(2) Liotta, L. F.; Di Carlo, G.; Pantaleo, G.; Deganello, G. *Appl. Catal., B* **2007**, *70*, 314.
(3) Llorca, J.; Homs, N.; Sales, J.; de la Piscina, P. R. *J. Catal.* **2002**, *209*, 306.
(4) Llorca, J.; Homs, N.; Sales, J.; Fierro, J.-L. G.; de la Piscina, P. R. *J. Catal.* **2004**, *222*, 470.
(5) Raróg-Pilecka, W.; Miśkiewiscz, E.; Matyszek, M.; Kaszkur, Z.; Kępiński, L.; Kowalczky, Z. *J. Catal.* **2006**, *237*, 207.
(6) Hadjiivanov, K.; Avreyska, V.; Tzvetkov, G.; Stefanov, P.; Chupin, C.; Mirodatos, C.; Marinova, Ts *Surf. Interface Anal.* **2001**, *32*, 175.
(7) Yung, M. M.; Holmgreen, E. M.; Ozkan, U. S. *J. Catal.* **2007**, *247*, 356.
(8) Lick, I. D.; Carrascull, A.; Ponzi, M.; Ponzi, E. N.; Botto, I. L *Mater. Chem. Phys.* **2005**, *92*, 327.
(9) Jansson, J.; Palmqvist, A. E. C.; Fridell, E.; Skoglundh, M.; Österlund, L.; Thormählen, P.; Langer, V. *J. Catal.* **2002**, *211*, 387.
(10) Fox, J. M., III *Catal. Rev.* **1993**, *35*, 169.
(11) Schulz, H. *Appl. Catal., A* **1999**, *186*, 3.
(12) van der Laan, G. P.; Beenackers, A. A. C. M. *Catal. Rev.* **1999**, *41*, 255.
(13) Khodakov, A. Y.; Chu, S; Fongarland, P. *Chem. Rev.* **2007**, *107*, 1692.
(14) Enache, D. I.; Rebours, B; Roy-Auberger, M.; Revel, R. *J. Catal.* **2002**, *205*, 346.
(15) Jacobs, G.; Das, T. K.; Zhang, Y.; Li, J.; Recoillet, G.; Davis, B. H *Appl. Catal., A* **2002**, *233*, 263.
(16) Tsubaki, N.; Sun, S.; Fujimoto, K. *J. Catal.* **2001**, *199*, 236.
(17) Ernst, B.; Libs, S.; Chaumette, P.; Kiennemann, A. *Appl. Catal., A* **1999**, *186*, 14.
(18) Girardon, J.-S.; Lermontov, A. S.; Gengembre, L.; Chernavskii, P. A.; Griboval-Constant, A.; Khodakov, A. Y. *J. Catal.* **2005**, *230*, 339.
(19) Kraum, M.; Baerns, M. *Appl. Catal., A* **1999**, *186*, 189.
(20) Rohr, F.; Lindvåg, O. A.; Holmen, A.; Blekken, E. A. *J. Catal.* **2000**, *58*, 247.
(21) Jongsomjit, B.; Panpranot, J.; Goodwin, J. G. *J. Catal.* **2003**, *215*, 66.
(22) Ali, S.; Chen, B.; Goodwin, J. G. *J. Catal.* **1995**, *157*, 35.

10.1021/cm8002657 CCC: $40.75
Published on Web 05/23/2008

and zirconia eases reduction of cobalt oxide.[23,24] Often enough, noble metals such as ruthenium are introduced as additives/promoters in small amounts, especially to materials with strong cobalt−support interactions. These noble metals facilitate the reduction of cobalt at lower temperature by the hydrogen spillover effect.[25] Because of its high hydrogenation activity, Ru could also inhibit carbon deposition on the cobalt surface and thus keep the active sites available for reaction.[26]

To optimize the usage of cobalt sites, it is essential to have a high surface area of the active metal. Ideally, this can be achieved by small cobalt size. Unfortunately, achieving this via the aforementioned traditional preparation techniques requires operation at low concentrations and hence is time-consuming. Here, the flame spray pyrolysis (FSP) aerosol technique as an alternative one-step method is used to prepare cobalt-based nanocomposites. Despite its rapid (milliseconds) synthesis, FSP is a versatile technique for synthesizing nanomaterials with closely controlled characteristics and of various complexities ranging from simple metal oxides,[27–31] noble metal/metal oxides,[29,32] metal oxides/metal oxides[30,33] to mixed-metal oxides.[34,35] Additionally, the technique has been demonstrated as an easily scalable technique even at pilot scales.[36–38]

In this work, the synthesis of a novel composite structure by FSP technique is presented, where a unique configuration of highly dispersed cobalt within a zirconia matrix is obtained. The incorporation of ruthenium as a promoter, also through the one-step technique, is studied and will be demonstrated as having a different role compared to the conventional impregnated cobalt. To gain a better understanding on the structural−catalytic properties of the flame-made composites, FT synthesis is chosen as the probe reaction because of its stringent requirement for active cobalt sites and its importance in energy applications. This is the first time materials of such kind are synthesized and assessed for potential catalysis. The structural and catalytic properties of FSP-made cobalt composites are also benchmarked to those prepared by incipient wetness impregnation,[15] a commonly accepted benchmark for FT catalysis.[14–19]

2. Experimental Section

2.1. Preparation of Composite Nanoparticles. A flame spray pyrolysis reactor[27] was used to synthesize cobalt oxide and cobalt-zirconia (20 wt % Co) composite nanoparticles. In the former, 0.5 M cobalt 2-ethylhexanoate (Aldrich, 65%) in xylene (Riedel deHaen, 96%) was used as the precursor. For the cobalt-zirconia composite, a mixture of 0.5 M zirconium(IV) propoxide (Aldrich, 70%) and 0.2 M cobalt 2-ethylhexanoate in xylene was prepared. Doping of Ru was carried out by the addition of ruthenium(III) acetylacetonate (Aldrich, 97%) to the precursor solutions. During FSP synthesis, the liquid precursor (1, 5, or 10 mL/min) was fed to the flame using a syringe pump (Inotech R232). The liquid was dispersed with 5 L/min oxygen (1.5 bar) at the nozzle tip to form fine spray droplets. Combustion of the droplets was initiated and supported by a surrounding oxy-methane flame (3.2 L/min O_2/1.5 L/min CH_4) forming a self-sustained main core flame. Additional 5 L/min of sheath oxygen was issued through the outermost ring. Product particles were collected on a glass fiber filter (Whatmann GF/D, 25.7 cm in diameter) with the aid of a vacuum pump (Alcatel SD Series). For mechanically mixed samples, the FSP-made cobalt oxide particles were mixed with commercial Nextech zirconia powder (com-ZrO_2, 8% yttria) in a polypropylene container loaded with ceramic balls (Armfield). The container with powder and ceramic balls was sealed and placed on a roller (Ratek) for 16 h. The powder soft aggregates were broken into smaller fractions to obtain an even mechanical mixture at interparticle level.

Reference materials were prepared by incipient wetness impregnation (IWI), following the procedure of Jacobs et al.[15] Aqueous cobalt nitrate (1.7 M, Aldrich) was added in 5 steps (10 mL of aliquot addition during each step) over precalcined (400 °C, 4 h) commercial Nextech yttria-stabilized zirconia (92% ZrO_2 and 8% Y_2O_3, 137 m^2/g) to give a total of 20 wt % Co. For convenience, the impregnated sample is denoted 20%Co/com-ZrO_2 throughout the manuscript. Drying procedure at 60 °C was carried out in a rotary evaporator following each impregnation step. Aqueous ruthenium(III) chloride hydrate (99.98%, Aldrich)[19,25,39,40] was added and further dried at the same condition in the rotary evaporator. The impregnated particles were calcined in air at 400 °C for 4 h.

2.2. Structural Characterization of Composite Nanoparticles. The specific surface area (SSA), adsorption isotherms, and pore size distribution of all materials were obtained by nitrogen adsorption at 77 K (Micromeritics Tristar 3000). Prior to analysis, the powders were pretreated in a Micromeritics VacPrep unit at 150 °C for at least 1 h to remove adsorbed water or volatile organics. X-ray diffraction (XRD) analysis of the powders was carried out on Siemens D5000 operated at 30 kV, 30 mA at 2θ (Cu $K\alpha$) = 20−80°, step width = 0.02°, and scan speed = 0.6°/min. Crystallite sizes of Co_3O_4 and ZrO_2 were estimated from Scherrer formula[41] at $[3\ 1\ 1]_{Co_3O_4}$ (2θ = 36.8°) and $[1\ 1\ 1]_{ZrO_2}$ (2θ = 30.6°) Bragg reflections, respectively, neglecting the effect of microstrain.[41,42] High-resolution transmission electron microscopy (HRTEM) was carried out on a Tecnai F30 microscope operating at 300 kV,

(23) Zhang, Y.; Shinoda, M.; Tsubaki, N. *Catal. Today* **2004**, *93−95*, 55.
(24) Enache, D. I.; Roy-Auberger, M.; Revel, R. *Appl. Catal., A* **2004**, *268*, 51.
(25) Kogelbauer, A.; Goodwin Jr., J. G.; Oukachi, R. *J. Catal.* **1996**, *160*, 125.
(26) Iglesia, E.; Soled, S. L.; Fiato, R. A.; Via, G. H. *J. Catal.* **1993**, *143*, 345.
(27) Mädler, L.; Stark, W. J.; Pratsinis, S. E. *J. Mater. Res.* **2002**, *17*, 1356.
(28) Teoh, W. Y.; Denny, F.; Amal, R.; Friedmann, D.; Mädler, L.; Pratsinis, S. E. *Top. Catal.* **2007**, *44*, 489.
(29) Teoh, W. Y.; Mädler, L.; Beydoun, D.; Pratsinis, S. E.; Amal, R. *Chem. Eng. Sci.* **2005**, *60*, 5852.
(30) Li, D.; Teoh, W. Y.; Selomulya, C.; Woodward, R. C.; Amal, R.; Rosche, B. *Chem. Mater.* **2006**, *18*, 6403.
(31) Li, D.; Teoh, W. Y.; Selomulya, C.; Woodward, R. C.; Munroe, P.; Amal, R. *J. Mater. Chem.* **2007**, *17*, 4876.
(32) Strobel, R.; Baiker, A.; Pratsinis, S. E. *Adv. Powder Technol.* **2006**, *17*, 457.
(33) Mädler, L.; Stark, W. J., W. J.; Pratsinis, S. E. *J. Appl. Phys.* **2002**, *92*, 6537.
(34) Schulz, H.; Mädler, L.; Pratsinis, S. E. *Adv. Funct. Mater.* **2005**, *15*, 830.
(35) Teoh, W. Y.; Amal, R.; Mädler, L.; Pratsinis, S. E. *Catal. Today* **2007**, *120*, 203.
(36) Mueller, R.; Mädler, L.; Pratsinis, S. E. *Chem. Eng. Sci.* **2003**, *58*, 1969.
(37) Mueller, R.; Jossen, R.; Pratsinis; S. E.; Watson, M.; Akhtar, M. K. *J. Am. Ceram. Soc.* **2004**, *87*, 197.
(38) Jossen, R.; Mueller, R.; Pratsinis, S. E.; Watson, M.; Akhtar, M. K. *Nanotechnology* **2005**, *16*, S609.
(39) Reinikainen, M.; Niemelä, M. K.; Kakuta, N.; Suhonen, S. *Appl. Catal., A* **1998**, *174*, 61.
(40) Hosseini, S. A.; Taeb, A.; Feyzi, F.; Yaripour, F. *Catal. Commun.* **2004**, *5*, 137.
(41) Scherrer, P. *Göttingen Nachrichten* **1918**, *2*, 98.
(42) Borg, O.; Eri, S.; Blekkan, E. A.; Storsæter, S.; Wigum, H.; Rytter, E.; Holmen, A. *J. Catal.* **2007**, *248*, 89.

equipped with energy-dispersive X-ray spectroscopy (EDX) and high-angle annular dark field (HAADF) for scanning transmission electron microscopy (STEM) imaging. Surface analysis of the composite materials was done by X-ray Photoelectron Spectroscopy (XPS) on ESCALab220i-XL (VG Scientific) using a monochromatised Al $K\alpha$ radiation at a pass energy of 20 eV and at $P < 2 \times 10^{-9}$ mbar. The energy scale was calibrated and corrected for charging by using the C1s (285.0 eV) line as the binding energy reference. Peak fittings and deconvolution was performed using the Eclipse (VG Scientific software), with peak ratio $Co2p_{1/2}$: $Co2p_{3/2}$ = 1:2 and ΔE ($Co2p_{1/2}$ − $Co2p_{3/2}$) was set to 15 eV.[43]

Temperature programmed reduction (TPR) of the powder samples were carried out by passing 38 mL/min of 5% H_2/He[19,21,24,25,42] at a 10°/min ramp (25−800 °C). Chemisorption of carbon monoxide (CO) was carried out on prereduced samples (at 38 mL/min of 5% H_2/He, 430 °C) by passing 26 mL/min of 2%CO/1%Ar/97%He through the samples at 25 °C. Cobalt dispersion (D_{Co} = ratio of the number of surface cobalt atoms to total cobalt atoms in the bulk) was calculated from the total CO chemisorbed assuming a CO/Co stoichiometric factor of 1.0.[19] All gases, both in TPR and CO-chemisorption experiments, were monitored using a mass spectrometer (Thermostar, Vacuum Pfeiffer).

2.3. Fischer−Tropsch Synthesis over Co-ZrO_2. As-prepared FSP-made cobalt-zirconia samples, mechanically mixed samples and impregnated reference materials were pressed into pellets (Ø ≈ 1 cm) followed by crushing and sieving into the 500−850 μm fraction. Accurately weighed sieved pellets (1.0 g) were diluted with additional inert α-Al_2O_3 (sieve diameter 500−850 μm) to make up 1.5 cm^3 catalyst bed volume. Prior to catalytic testing, the pellets were first reduced slowly under 100 mL/min (Gas hourly space velocity, GHSV = 4000 h^{-1}) of 3% H_2 in N_2 at 260 °C and 1 bar for 24 h. It was then further reduced in 100 mL/min (GHSV = 4000 h^{-1}) of pure H_2 at the same temperature and pressure for another 16 h. FT reaction was carried out by introducing 60 mL/min (GHSV = 2400 h^{-1}) of CO:H_2:N_2 reactant feed gas in the ratio of 2:3:1, respectively. The FT reaction was maintained at 215 °C and 20 bar.

3. Results and Discussion

3.1. Structural Properties of Cobalt−Zirconia. Flame spray pyrolysis of zirconium propoxide/xylene liquid precursor yielded ZrO_2 nanoparticles of predominantly tetragonal phase (open circle, Figure 1) with a small amount of monoclinic phase, in agreement with the earlier ZrO_2 synthesis by FSP.[37,44,45] During the FSP, dispersed precursor droplets are combusted to form Zr vapor within the flame. As the flame gets cooler downstream, nucleation of fine ZrO_2 takes place because of supersaturation. This is followed by the growth phase where the ZrO_2 nuclei undergo sintering, coalescence, aggregation and agglomeration, before leaving the flame. The addition of 20% (w/w) cobalt through incorporation of cobalt 2-ethylhexanoate in the liquid precursor resulted in the transformation to ZrO_2 cubic phase (solid

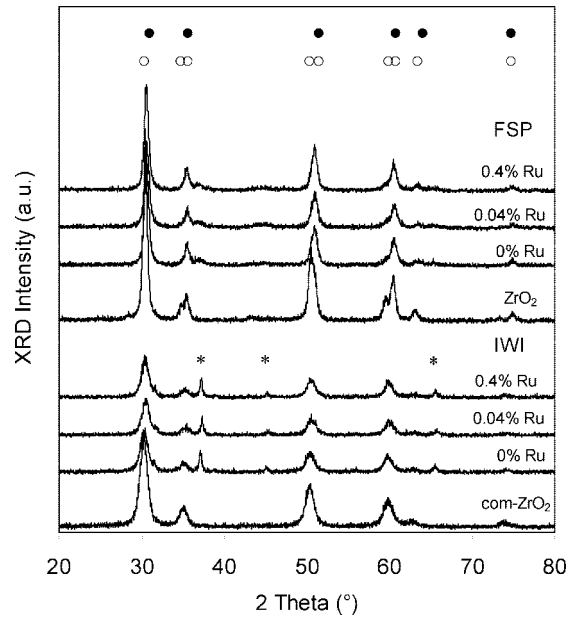

Figure 1. XRD spectra of FSP-made and reference-impregnated (IWI) composite materials. Except for FSP ZrO_2 and com-ZrO_2, all samples consist of 20% Co-ZrO_2 (Co exists as Co_3O_4). The open (○) and solid (•) circles are the characteristic peaks of tetragonal and cubic ZrO_2, respectively, whereas the asterisks (*) denote the characteristic peaks of cubic Co_3O_4.

circle, Figure 1). This could be attributed to the phase stabilization of ZrO_2 by the cubic phase Co_3O_4,[46] indicating strong Co_3O_4−ZrO_2 interactions. Note that the amount of cobalt loading (equivalent to 34 at %) in the present study far exceeds the solubility limit of <10 at %.[46] Hence, it would be expected that phase segregation of Co_3O_4 takes place at such high loading. From the XRD pattern in Figure 1, only a weak Bragg reflection at $2\theta = 36.8°$ belonging to cubic Co_3O_4 [3 1 1] phase could be observed for the FSP-prepared samples suggesting that most of the Co_3O_4 is present in highly dispersed form. As will be shown later, a more sensitive technique of X-ray photoelectron spectroscopy (XPS) was employed to confirm the presence of surface Co_3O_4 crystals. The low XRD signal of Co_3O_4 coupled with the overlapping of cubic ZrO_2 [2 0 0] peak ($2\theta = 35.5°$) was too small for accurate crystallite size determination.

For the reference composite materials prepared by incipient wetness impregnation (IWI) of cobalt nitrate on commercial zirconia (com-ZrO_2, Nextech), a small but sharp Co_3O_4 reflection ($2\theta = 36.8°$) is clearly evident in the XRD patterns (Figure 1). These reference materials are comparable to other similarly made supported Co catalysts reported in the literature as will be verified later (section 3.4). Like the FSP-made ZrO_2, com-ZrO_2 powder consisted of mainly tetragonal phase. However, unlike the cubic phase stabilization observed in FSP samples, the tetragonal phase remains even after impregnation with cobalt. Nevertheless, XRD intensities of the characteristic ZrO_2 Bragg reflections in impregnated samples were significantly reduced compared to pristine zirconia. The effect is not due to peak broadening effect, as the Scherrer-determined ZrO_2 crystallite sizes remained the

(43) Moulder, J. F., Stickle, W. F., Sobol, P. E., Bomben, K. D., *Handbook of X-ray Photoelectron Spectroscopy*; Chastain, J., Ed.; Perkin-Elmer Corporation: Eden Prairie, MN,1992.
(44) Stark, W. J.; Maciejewski, M.; Mädler, L.; Pratsinis, S. E.; Baiker, A. *J. Catal.* **2003**, *220*, 35.
(45) Jossen, R.; Heine, M.; Pratsinis, S. E.; Akhtar, M. K. *Chem. Vap. Deposition* **2006**, *12*, 614.
(46) Wu, P.; Kershaw, R.; Dwight, K.; Wold, A. *Mater. Res. Bull.* **1988**, *23*, 475.

Table 1. Overview of Physicochemical Properties of Cobalt-Zirconia Prepared by FSP, IWI (reference), and Mechanical Mixing

	Ru content (%)	SSA (m^2/g)	d_{ZrO_2}[a] (nm)	$d_{Co_3O_4}$[a] (nm)	d_{Co}[b] (nm)	% reduction	D_{Co}[c] (%)
FSP							
ZrO_2	0	73	15	-	-	0	0
20%Co−ZrO_2	0	82	12	-	36	65	1.7
0.04%Ru−20%Co−ZrO_2	0.04	75	12	-	12	59	4.6
0.4%Ru−20%Co−ZrO_2	0.4	64	13	-	9	63	6.6
0.4%Ru−20%Co−ZrO_2[d]	0.4	178	7	-	12	62	4.9
IWI							
com-ZrO_2	0	137	8	-	-	0	0
20%Co/com-ZrO_2	0	92	8	23	15	87	5.6
0.04%Ru−20%Co/com-ZrO_2	0.04	85	7	28	14	89	6.3
0.4%Ru−20%Co/com-ZrO_2	0.4	87	7	25	15	91	5.9
Mechanical							
20%Co + com-ZrO_2[e]	0	38	8	15	24	76	3.0
20%Co + com-ZrO_2	0	101	8	11	25	79	3.1
0.4%Ru−20%Co + com-ZrO_2	0.4	107	8	11	26	76	2.8

[a] Crystallite sizes were estimated by the Scherrer formula. [b] Metallic cobalt size was measured from dispersion, D_{CO}(%) and % reduction given by eq E1 in the Supporting Information. [c] Cobalt dispersion calculated assuming stoichiometric CO:Co = 1.[15] [d] Prepared at precursor feed flowrate = 1 mL/min. Unless stated otherwise, all FSP and mechanically mixed catalysts were prepared at 5 mL/min. [e] Prepared at precursor feed flowrate = 10 mL/min.

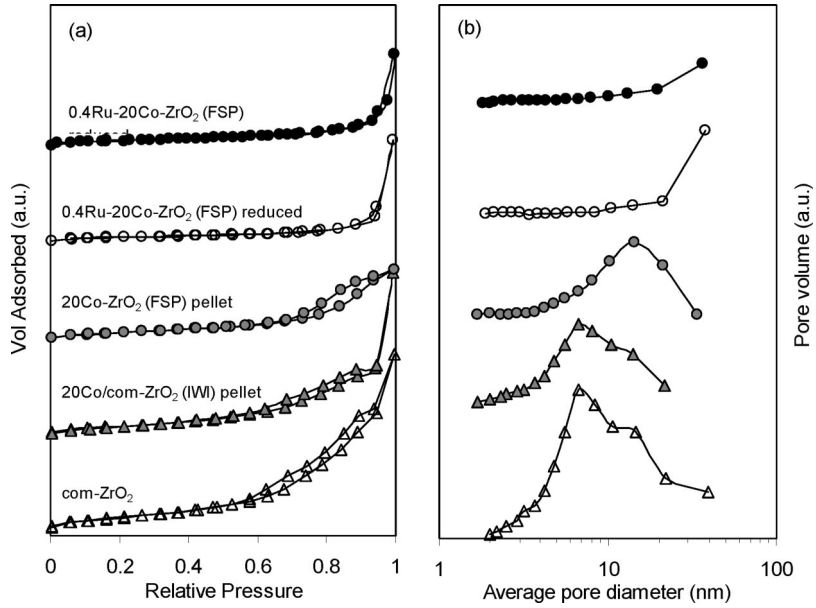

Figure 2. (a) Adsorption−desorption isotherm of various samples prepared by IWI and FSP and (b) the corresponding pore size distribution. Unless otherwise stated, the samples were nonpelletized (as-prepared powder).

same as before impregnation (Table 1). The reduction in the intensities of ZrO_2 reflection is attributed to the X-ray attenuation of Co_3O_4, where the ZrO_2 signal is shielded from surface-deposited Co_3O_4.[47] Because Co_3O_4 is mainly deposited on the zirconia surface without altering the structure of ZrO_2, no changes in ZrO_2 reflection positions were observed (Figure 1). The crystallite sizes of Co_3O_4 were ∼25 nm and unaffected by addition of Ru even up to 0.4 wt % (Table 1).

The presence of Ru was invisible in all the XRD patterns (both FSP and IWI) shown in Figure 1 as a result of low metal loading (0.04 and 0.4% w/w Ru) and more importantly its high dispersion. Addition of Ru did not affect crystallite sizes and surface areas of Co−ZrO_2 during FSP preparation (Table 1). The surface of as-prepared FSP materials was nonporous, as typically observed for flame-made particles[48] and also indicated by the type II N_2 adsorption isotherm (solid dark circles, Figure 2). Only large pores >20 nm were observed originating from the interaggregate pores. The interaggregate pore size was reduced (∼15 nm) upon pelletization due to close packing of primary particles, giving rise to the hysteresis in type IV adsorption−desorption isotherm (gray circle, Figure 2).

Further morphological characterisations on the Co_3O_4−ZrO_2 particles were carried out by TEM. Figure 3. shows that the FSP particles were made up of homogeneous crystalline particles of ∼13 nm diameter, in qualitative agreement with the Scherrer-determined crystallite size (Table 1). From the STEM-EDX elemental analysis on various areas of the samples, no distinct segregation of Co and Zr oxide crystals could be observed. In all cases, almost identical Zr/Co signal ratios were obtained on individual particles or a cluster of particles (Figures 3d−f). This strongly corroborated the XRD analysis on the formation of finely dispersed Co_3O_4 in ZrO_2 matrix. As with XRD analysis, the low amount of Ru addition renders a negligible signal even when inspected by EDX.

(47) Hubbell, J. H. *Int. J. Appl. Radiat. Isot.* **1982**, *33*, 1269.
(48) Pratsinis, S. E. *Prog. Energy Combust. Sci.* **1998**, *24*, 197.

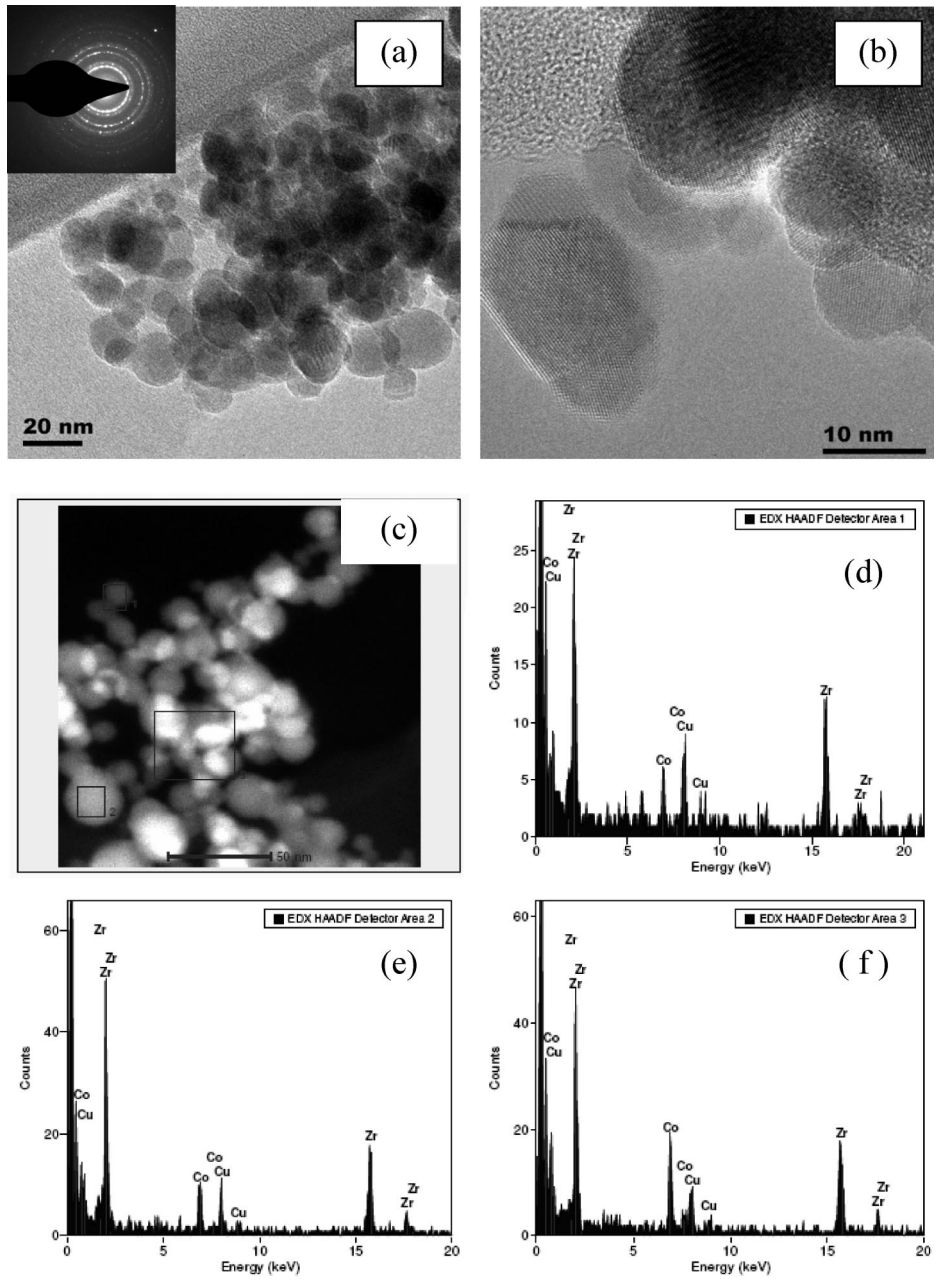

Figure 3. HRTEM (a,b) and STEM (c) of as-prepared FSP 0.4%Ru−20%Co-ZrO_2 (Co exists as Co_3O_4). Also shown are the EDX spectra (d−f) of points analysis taken at selected spots in (c), showing the homogeneous distribution of Co and Zr in the particle. The Cu signals originate from the TEM copper grids.

In contrast to the FSP-made samples, the reference impregnated materials consisted of irregular Co_3O_4 (<200 nm, Figure 4) deposited on the heavily agglomerated fine zirconia particles (d_{ZrO_2} = 7−8 nm, Table 1), as confirmed by EDX (Figure 4d−f). The large discrepancy between the TEM size of Co_3O_4 and that determined by XRD (25 nm) indicates that the Co_3O_4 clusters are made up of small Co_3O_4 nanocrystals. Formation of large and porous Co_3O_4 clusters by incipient impregnation technique is commonly observed and reported on other supports such as Al_2O_3,[49] TiO_2 and SiO_2.[50] Besides the usual metal-support interaction, support pore size was thought to have extensive influence on the cluster size.[50–52] The small interparticle pores of com-ZrO_2 (pore diameter = 6.7 nm) (Figure 2), resulted in the formation of large Co_3O_4 clusters due to migration and diffusional growth of Co_3O_4 across pores during calcinations.[50,51]

The structure of the cobalt oxides was further investigated by surface sensitive XPS analysis. Figure 5 shows the typical $Co2p_{3/2}$ (peak 780.3 eV) and $Co2p_{1/2}$ (peak 795.3 eV) binding energies corresponding to Co_3O_4 for both FSP-made and impregnated reference materials. The Co2p signals were further resolved into Co^{III} (tetrahedral)

(49) Li, P.; Liu, J.; Nag, N.; Crozier, P. A. *Appl. Catal., A* **2006**, *307*, 212.
(50) Storsæter, S.; Tøtdal, B.; Walmsley, J. C.; Tanem, B. S.; Holmen, A. *J. Catal.* **2005**, *236*, 139.
(51) Castner, D. G.; Watson, P. R.; Chan, I. Y. *J. Phys. Chem.* **1989**, *93*, 3188.
(52) Feller, A.; Claeys, M.; van Steen, E. *J. Catal.* **1999**, *185*, 120.

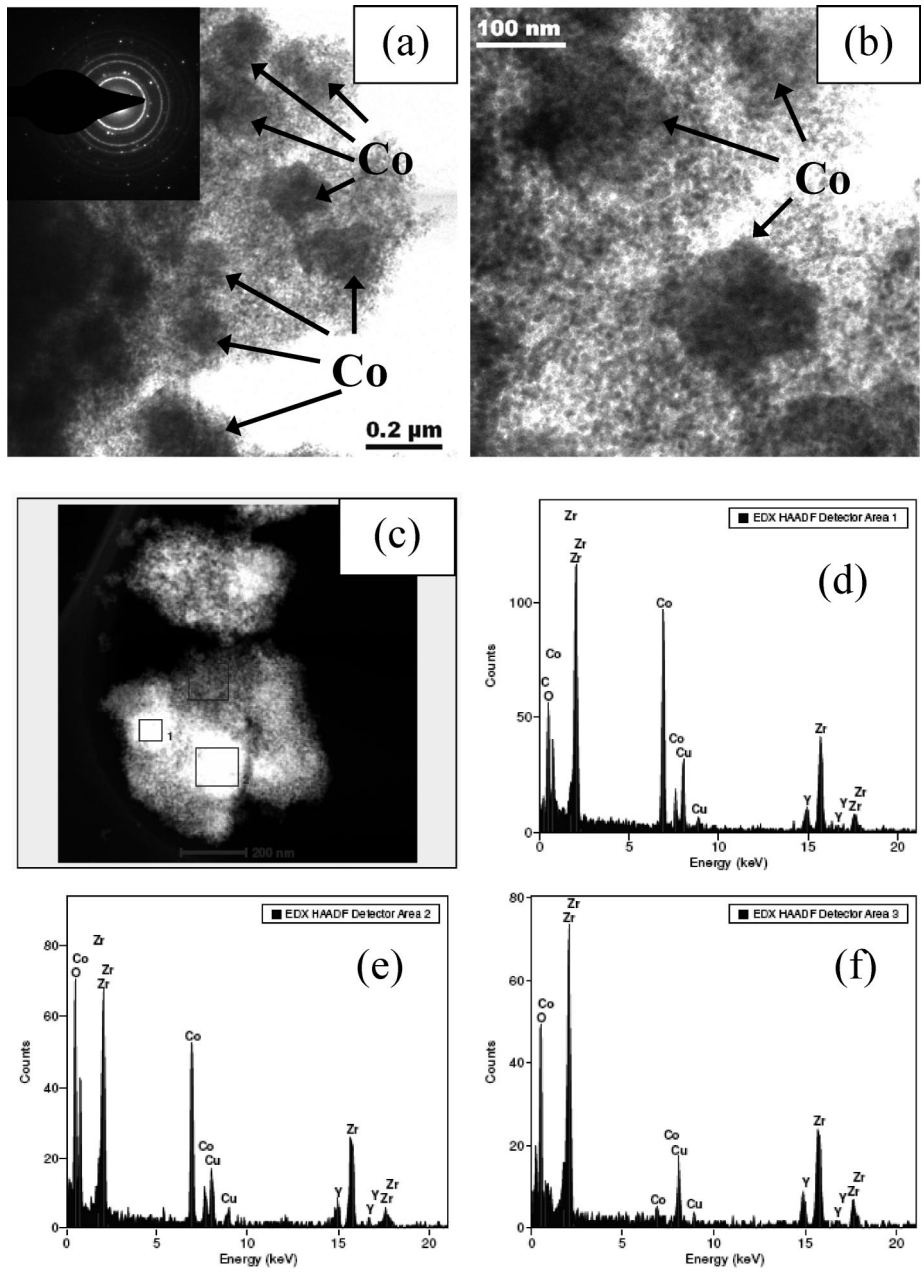

Figure 4. HRTEM (a, b) and STEM (c) of as-prepared IWI 0.4%Ru−20%Co/com-ZrO_2 (Co exists as Co_3O_4). Also shown are the EDX spectra (d−f) of points analysis taken at selected spots in (c), showing that Co_3O_4 exists as large porous clusters deposited on com-ZrO_2. The Cu signals originate from the TEM copper grids.

and Co^{II} (octahedral) as shown in Figure 5 and Table 2 and in agreement with the literature.[17,53] Under the XPS, the ratio of Co^{III} and Co^{II} is similar for the FSP and IWI samples despite Co_3O_4 being invisible in the former XRD spectra as a result of its high dispersion. Additionally, Ru which was previously undetected by XRD and TEM, was determined by XPS to exist as Ru(II) oxide from the $3d_{5/2}$ peak at binding energy of 282.1 eV.

Apart from determining the oxidation state of the surface elements, the surface elemental composition of Co, Zr, and Ru was also calculated from the XPS surface element quantification. Despite the formation of highly dispersed Co_3O_4 in ZrO_2 matrix prepared by FSP, the distribution of Co may not be perfectly uniform, as illustrated in the difference in relative surface elemental composition between nominal and surface Co/Zr ratios (Table 2). Some segregation of Co may have occurred within the ZrO_2 matrix leading to lower surface Co/Zr ratio (0.39) than the nominal value (0.52). This is similar to our previous investigation of FSP-made Fe-TiO_2 where at high Fe/Ti ratio (>5%), a lower surface Fe/Ti ratio than that of bulk (nominal) was observed due to elemental segregation.[35] The segregation observed here stems from the high Co loading which exceeded the solubility limit at which the two phases (Zr and Co oxides) exist in perfect homogeneity. Nevertheless, the segregation is only restricted to the intraparticle level as probed by STEM-EDX (Figure 3d−f). As for the case of reference impregnated samples, the formation of large Co_3O_4 clusters on fine zirconia (Figure 4) resulted in a much lower Co/Zr ratio (almost twice lower than that of FSP, Table 2). A significant portion of Co_3O_4 content is embedded beneath

(53) Sexton, B. A.; Hughes, A. E.; Turney, T. W. *J. Catal.* **1986**, *97*, 390.

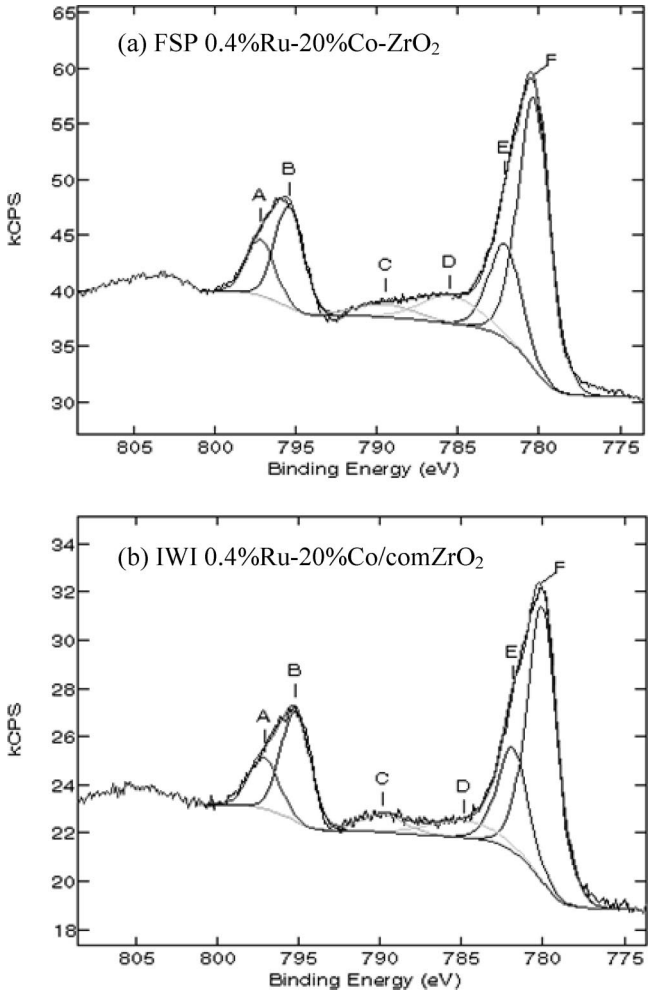

Figure 5. XPS Co $2p_{3/2}$ peak of as-prepared 0.4%Ru−20%Co-ZrO_2 made by (a) FSP- and (b) IWI. The deconvoluted peaks shown in the spectra are labeled (A) Co^{II} $2p_{1/2}$, (B) Co^{III} $2p_{1/2}$, (C) Co^{II} satellite peak, (D) Co^{III} satellite peak, (E) Co^{II} $2p_{3/2}$, and (F) Co^{III} $2p_{3/2}$.

the cluster surface and as a result was not detected by XPS. Note that the specific surface areas of the two samples analyzed by XPS (Figure 5) are comparable, with 64 (FSP) and 87 (IWI) m^2/g (Table 1), hence allowing for reasonable direct comparisons between the elemental ratios and the absolute surface quantity of each element.

Enrichment of Ru on the impregnated cobalt surface is also evident, as indicated by the higher Ru/Co ratio (3.25%) than that of nominal (1.16%) shown in Table 2. The findings agree well with the observation by Iglesia et al.[26] on Ru−Co/TiO_2 composites, also prepared by impregnation. Although the surface and nominal Ru/Zr ratios are very similar, it is unlikely for Ru to be embedded and distributed within the bulk of com-ZrO_2 support given the nature of the preparation method, as supported by the unchanged crystallography of the zirconia. In other words, Ru should be concentrated either on the zirconia or Co_3O_4 surface. The former would have resulted in significant higher surface Ru/Zr ratio than that of nominal, which is not the case (Table 2). Hence it is more likely that Ru is enriched, or at least in the proximity of Co surface, which in turn is mostly embedded in the porous clusters and as such not detected in significant surface amount relative to Zr. It was also suggested that an intimate contact between impregnated Co and Ru could form during calcination of the bimetallic precursors at 400 °C,[26] a condition similar to the reference materials prepared here by IWI.

The interpretation of surface Ru composition on FSP composite samples is less straightforward due to the uncertainty in the location of Ru within the particle, be it specifically within the Co or Zr matrix or even isolated on the particle surface. As shown in Table 2, surface enrichment of Ru relative to Co in FSP-made composite particles (2.02%) is only slightly higher than the nominal composition. The higher Ru/Co ratio can be understood since it is known that there was less Co on the surface than in bulk, as discussed earlier. Also, because Co/Zr (39%) and Ru/Zr (0.79%) ratios were in opposite directions to the corresponding nominal ratios of 52 and 0.61%, respectively, it can be reasonably deduced at this stage that the distribution of Ru is not dictated by that of Co. However, there are still two possible simplified scenarios: (1) Ru enrichment on FSP Co_3O_4−ZrO_2 surface or (2) homogeneous distribution of Ru in ZrO_2 matrix. Judging from the rather similar surface and nominal Ru/Zr ratios (Table 2), it is very likely that Ru is uniformly distributed within the cobalt−zirconia particles. The distribution of Ru in the particle bulk is a key parameter leading to the significant enhancement in Co reducibility as presented in the next section.

3.2. Reducibility of Cobalt−Zirconia Nanocomposites. In all FSP-made and impregnated cobalt−zirconia particles, a two-step reduction was observed (Figure 6). The result is consistent with the trend generally observed on supported Co_3O_4 materials[15,19,25,40,54–56] and corroborates the fact that Co exists as Co_3O_4 both on FSP and impregnated samples (Figure 5 and Table 2). The first reduction peak is ascribed to the reduction of Co_3O_4 to CoO (eq 1), whereas the second involves further reduction to metallic Co (eq 2)

$$Co_3O_4 + H_2 \rightarrow 3CoO + H_2O \quad (1)$$

$$3CoO + 3H_2 \rightarrow 3Co^0 + 3H_2O \quad (2)$$

All the particles (FSP and IWI) exhibited close to the stoichiometric 3 times more H_2 consumption in the second peak than the first, i.e., in agreement with eqs 1 and 2. In the absence of Ru, the relatively high reduction temperature of FSP-made cobalt−zirconia (Table 1 and Figure 6) is attributed to the small cobalt size and the strong interaction of cobalt with the support matrix. A distinct dual hydrogen consumption hump is also observed on the first peak of FSP sample, the first being surface Co(III), whereas the second hump originates from the embedded Co(III). The embedded Co(III) can be partially reduced even in the absence of Ru, but requires much higher temperature (Figure 6). High reduction temperature was required to overcome the high surface energy attributable to the dispersed Co_3O_4 clusters stabilized by the ZrO_2 matrix (strong cobalt−zirconia interaction).[55,57,58]

(54) Liu, Y.; Chen., J.; Fang, K.; Wang, Y.; Sun, Y. *Catal. Commun.* **2007**, *8*, 945.
(55) Liu, Y.; Fang, K.; Chen, J.; Sun, Y. *Green Chem.* **2007**, *9*, 611.
(56) Chernavskii, P. A.; Lermontov, A. S.; Pankina, G. V.; Torbin, S. N.; Lunin, V. V. *Kinet. Catal.* **2002**, *43*, 268.
(57) van Steen, E.; Claeys, M.; Dry, M.; Viljoen, E.; van de Loosdrecht, J. L.; Visagie, J. L. *J. Phys. Chem. B* **2005**, *109*, 3575.
(58) Saib, A. M.; Borgna, A.; van de Loosdrecht, J.; van Berge, P. J.; Geus, J. W.; Niemantsverdriet, J. W. *J. Catal.* **2006**, *239*, 326.

Table 2. XPS Binding energies of Co_3O_4, ZrO_2 and RuO, and also the relative surface composition of the elements

	XPS binding energies (eV)						
	Co 2p3/2				surface elemental ratios (%)		
	Co(III)	Co(II)	Zr 3d5/2	Ru 3d5/2	Co/Zr	Ru/Co	Ru/Zr
nominal					52.23	1.16	0.61
0.4%Ru−20%Co−ZrO_2 (FSP)	780.3	782.1	182.0	282.2	39.37	2.02	0.79
0.4%Ru−20%Co/com−ZrO_2 (IWI)	780.0	781.9	182.2	282.0	20.70	3.25	0.67

Although the reference impregnated materials exhibited low surface Co loading as measured by XPS, lower reduction temperatures could be achieved. This arises largely from the inherently different physical structure of cobalt in impregnated samples compared to FSP ones. In particular, the Co_3O_4 particles are present on the surface (easily accessible by H_2) and thus not stabilized by the ZrO_2 matrix. The distinct dual humps in the first reduction peak were not observed for impregnated samples in the absence embedded cobalt species. Perhaps also important to reiterate is the easier reduction of large Co_3O_4 crystallite sizes (23−28 nm, Table 1), not only in the reduction step to Co(II) but also toward Co^0 (eq 2).[55,58]

As a general trend, the addition of small amounts of Ru, 0.04 and 0.4%, in all FSP and impregnated materials significantly lowers the reduction temperature (Figure 6). For the impregnated samples, this is attributed to the H_2 spillover effect where atomically adsorbed hydrogen on Ru is easily transferred to the neighboring cobalt oxide.[59] Reduction of the minute amount of Ru is negligible in this case and is insufficient to account for the large amount of H_2 consumed by cobalt during TPR.[26] Hence, the extent of H_2 consumption can be reasonably attributed to the reduction of Co species. The dual-step H_2 consumption at a stoichiometric ratio of 1:3 for reduction of Co_3O_4 confirms this assumption.

Because of its novel structure, the role of Ru in the FSP-made cobalt−zirconia particles is different from the impregnated samples, resulting in a drastic enhancement in reduction temperature ($T_{reduction}$ maxima of second peak of 480 and 360 °C for 0 and 0.4% Ru loading, respectively). The large 120 °C shift is a drastic improvement in terms of reducibility compared to the undoped Co−ZrO_2 sample despite having similar structure. As was characterized earlier, the bulk of Co and Ru content is beneath the nonporous particle surface. Further characterization by N_2 adsorption−desorption and XPS on reduced samples did not reveal any change in structure (e.g., formation of surface pores, Figure 2, open circle) or enhancement in surface Co or Ru content, respectively, hence eliminating the possibility of easier reduction originating from enhanced surface Co or Ru. In other words, doping with Ru in FSP-made composites promoted not only the surface reducibility but particularly the bulk (embedded) Co species. The ease in reducing bulk Co with increasing Ru loading further resulted in the gradual merge of the two humps during the first reduction step as seen in Figure 6a.

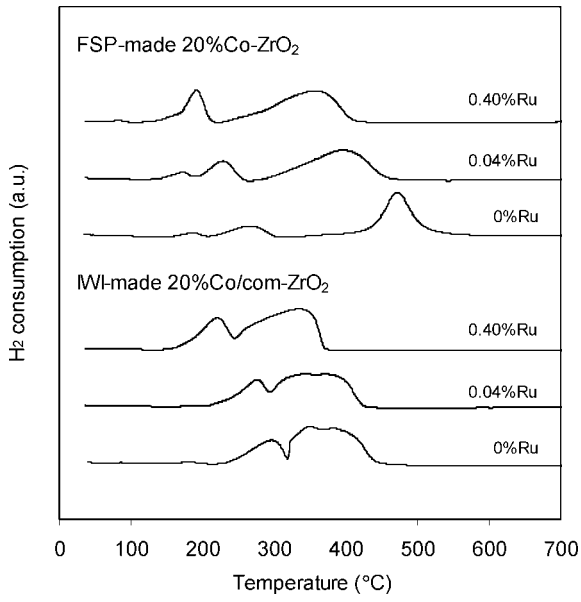

Figure 6. TPR profile of bare and Ru-doped Co−ZrO_2 prepared by (a) FSP and (b) IWI techniques.

3.3. Cobalt Dispersion of Reduced Cobalt−Zirconia Composites. The addition of Ru promoter improved not only the reducibility of FSP-made composites but led to a significant improvement in the amount of chemisorbed CO. CO atom adsorbs perpendicular to cobalt surface by bonding through C atom with binding energies ranging from 100−145 kJ/mol.[60] The cobalt dispersion as determined by CO chemisorption, D_{Co}, increased from 1.72 to 6.61% just by addition of 0.4% Ru (Table 1). No presence of CO chemisorption on both FSP-made ZrO_2 and com-ZrO_2 supports was detected. Because no formation of surface pores or migration of embedded Co to particle surfaces took place upon reduction (as discussed in section 3.2 and Figure 2), it is unlikely that CO molecules could be transferred to the Co sites beneath the nonporous ZrO_2 surface. Therefore, the presence of Ru was critical in enhancing the reducibility of Co at mild conditions (low reduction temperatures) resulting in the maintenance of the high Co dispersion (small metallic cobalt size, d_{Co}, Table 1). As an additional validation, CO_2 was not formed during CO chemisorption experiments, eliminating the possibility by catalytic oxidation of Ru. Enhancement in the specific surface area of 0.4% Ru-doped Co−ZrO_2 (from 64 to 178 m^2/g) through synthesis of smaller particles by FSP using a lower precursor feed flowrate of 1 mL/min did not enhance CO chemisorption even though more surface Co sites are now available. The decreased precursor feed flowrate resulted in lower temperature, shorter flame residence time and decreased metal concentrations which in turn suppressed the growth of particles (larger surface area). In fact, the D_{Co} values decreased from 6.6 to 4.9%, when the particle surface area was increased (Table

(59) Li, J.; Jacobs, G.; Zhang, Y.; Das, T.; Davis, B. H. *Appl. Catal., A* **2002**, *223*, 195.
(60) Kapiloff, E.; Ervin, K. M. *J. Phys. Chem. A* **1997**, *101*, 8460.

Table 3. Fischer−Tropsch Activity and Product Selectivity of Bare and Ru-Doped 20%Co-ZrO_2 Catalysts Prepared by Different Techniques[a]

	X(CO)[b]	$R_{integral}$	$TOF_{integral}$	Selectivity			χ^c
	%	(10^{-6} mol $s^{-1}g^{-1}$ cat)	(10^{-2} s^{-1})	C^1	C_2-C_4	C_{5+}	(10^{19} m^{-1})
FSP							
20%Co-ZrO_2	17.3	2.3	4.00	1.0	1.5	97.5	0.63
0.04%Ru-20%Co-ZrO_2	42.6	5.8	3.67	2.8	7.0	90.2	1.22
0.4%Ru-20%Co-ZrO_2	57.9	7.8	3.49	0.7	3.0	96.3	1.32
0.4%Ru-20%Co-ZrO_2[d]	41.7	5.6	3.41	2.4	10.6	87.0	0.95
IWI							
20%Co/com-ZrO_2	49.0	6.6	3.48	1.4	10.5	88.1	2.03
0.04%Ru-20%Co/com-ZrO_2	57.5	7.8	3.64	1.4	7.5	91.0	2.02
0.4%Ru-20%Co/com-ZrO_2	45.2	6.1	3.03	0.7	6.4	92.9	1.96
Mechanical							
20%Co + com-ZrO_2[e]	28.6	3.9	3.79	0.8	10.8	88.4	2.68
20%Co + com-ZrO_2	24.4	3.3	3.17	1.1	10.6	88.3	1.08
0.4%Ru-20%Co + com-ZrO_2	29.8	4.0	4.32	0.7	5.4	94.0	0.55

[a] Experimental conditions: 215°C, 20 bar, $H_2/CO = 1.5$, GHSV = 2400 h^{-1}, syngas flowrate = 3.6 L h^{-1} g_{cat}^{-1}. [b] Measured CO conversion. [c] Catalyst structural parameter calculated from eq E6 in the Supporting Information. [d] Prepared at precursor feed flowrate = 1 mL/min. Unless stated otherwise, all FSP and mechanically mixed catalysts were prepared at 5 mL/min. [e] Prepared at precursor feed flowrate = 10 mL/min.

1). This may partly be due to the enhanced intimate cobalt−zirconia interactions in finer samples.

The addition of Ru to reference impregnated samples has little influence on D_{Co} (Table 1). Tsubaki et al.[16] also reported little influence of Ru on Co dispersion of impregnated Ru−Co/SiO_2. Similarly, addition of Ru to mechanically mixed (Co_3O_4 + ZrO_2) samples, where direct cobalt-zirconia interaction is absent, did not result in improved Co dispersion (Table 1). Therefore the d_{Co} in both impregnated and mechanically mixed materials vary little with or without Ru dopant. Interestingly, despite the mechanically mixed samples having smaller d_{Co_3O4} than that of impregnated samples, the former resulted in larger d_{Co} than the latter upon reduction (Table 1). This is consistent with the more pronounced cobalt sintering in the mechanically mixed materials in the absence of metal−support interactions.

To this stage, it can be seen that Ru doping imparts a significant extent of cobalt reducibility and dispersion on FSP samples. The effects of Ru doping in the flame-made composite materials are inherently different from commonly observed in impregnated samples. Despite the apparently "undesirable" structure of embedded cobalt in FSP Co-ZrO_2, doping with uniformly distributed Ru within the bulk particle promoted the surface and bulk cobalt reducibility while also enhancing its dispersion. These characteristics make the FSP composite materials extremely desirable for FT reaction as will be discussed in the following section.

3.4. Comparisons of FSP and Impregnated Co−ZrO_2 in Fischer−Tropsch synthesis. In the absence of Ru promoter, the FSP-made cobalt-zirconia composite particles exhibited a low CO conversion rate (17.3%, $R_{integral}$ = 2.3 mol s^{-1} g^{-1}_{cat}) (Table 3). This can be attributed to the small amount of metallic Co available, as demonstrated during CO chemisorption measurements, due to cobalt stabilization in the ZrO_2 matrix. However, upon addition of 0.04 and 0.4% Ru, the conversion rates ($R_{integral}$ or cobalt-time yield) were increased by a factor of 2.5 and 3.4, respectively. This corresponded to a factor increase of 2.7 and 3.8, respectively (Table 1), with respect to the number of metallic Co sites available (D_{Co}). The data followed a linear relationship between CO conversion rates and the number of metallic Co (active) sites (Figure 7), conforming the trend reported by Iglesia et al.[26] This is true even for the nonpromoted Co-

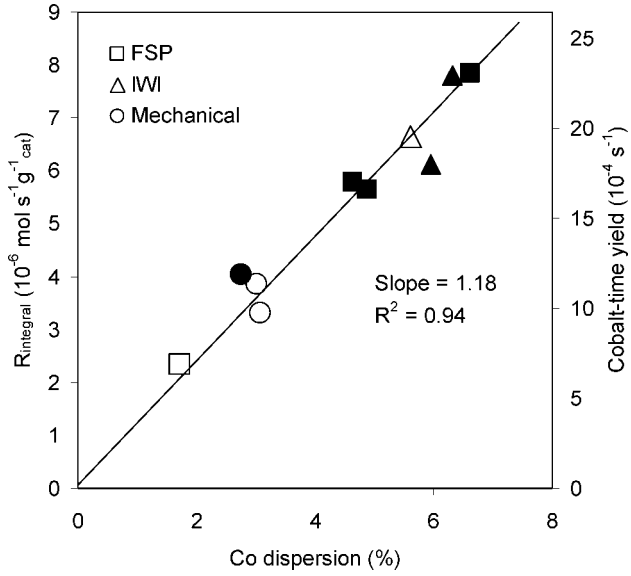

Figure 7. Effect of cobalt dispersion on the rate of CO conversion and cobalt time yield for differently prepared (FSP, IWI, and mechanical mixing) bare (open symbols) and Ru-doped (solid symbols) 20%Co-ZrO_2.

ZrO_2, where cobalt was only reduced at higher temperature leading to lower dispersion. Therefore, the conversion rate depends only on the number of metallic cobalt sites on the surface. Taking the basis of the number of Co active sites for each sample (estimated from CO-chemisorption on prereduced samples, see section 2.2), the turnover frequency (TOF) ranges between 0.034 and 0.040 s^{-1} (Figure 8). Similar values have also been reported in the literature for cobalt particles size >6 nm.[61]

The catalytic performance of FSP materials was compared with differently prepared materials. As shown in Figures 7 and 8, the data of mechanically mixed pure and Ru-doped Co_3O_4 particle (38−107 m^2/g) samples fall within the linearity of the FSP composite materials data. Despite the strong difference in physicochemical properties (surface areas and Ru promoter) within these unsupported samples, no significant difference in cobalt dispersion (2.8−3.1%, Table

(61) Bezemer, G. L.; Bitter, J. H.; Kuipers, H. P. C. E.; Oosterbeek, H.; Holewijn, J. E.; Xu, X.; Kapteijn, F.; van Dillen, A. J.; de Jong, K. P. *J. Am. Chem. Soc.* **2006**, *128*, 3956.

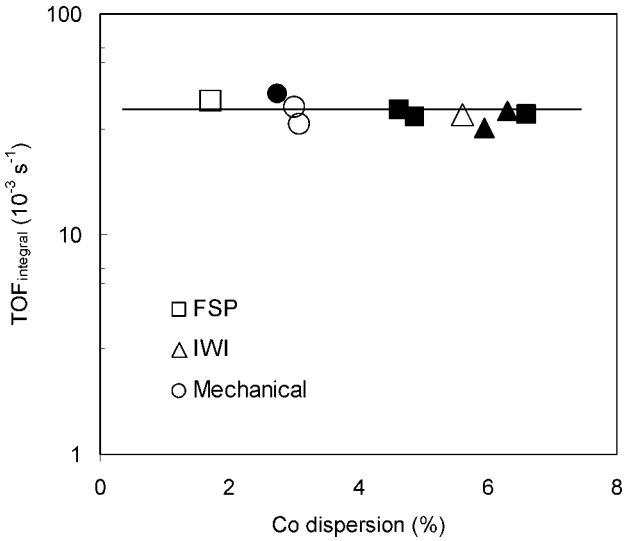

Figure 8. Effect of cobalt dispersion on the Fischer−Tropsch turnover frequency (TOF), based on CO conversion, for differently prepared (FSP, IWI, and mechanical mixing) bare (open symbols) and Ru-doped (solid symbols) 20%Co-ZrO_2.

1) was measured. Hence the CO conversion rates were also comparable ($R_{integral}$ = 3.3 − 4.0 mol s^{-1} g^{-1}_{cat}), but only less than half the conversion rate of the optimal FSP-made materials.

For the impregnated Co/com−ZrO_2 samples, the expected linear relationship between CO conversion rates and cobalt dispersion is still observed (Figure 7). Nevertheless, the enhancement in conversion rates between undoped and Ru-doping was less pronounced compared to that in FSP-made composite samples. As described in section 3.3, the D_{Co} in impregnated samples was only slightly affected by the doping of Ru promoter. Similar $TOF_{integral}$ values (0.030−0.036 s^{-1}) for the doped and undoped impregnated samples were also found. This again demonstrates that mainly the number of metallic cobalt sites on the surface is important, which is the highest for Ru-doped FSP and impregnated samples (due to its highest dispersion). The TOF values of Ru-doped samples are further in agreement with the results of Kogelbauer et al.[25] on similarly impregnated catalysts.

Since all the samples (FSP, IWI, and mechanically mixed samples) fall within a strict linear relationship as shown in Figure 7, an average $\langle TOF_{integral} \rangle$ = 0.035 s^{-1} (see the Supporting Information, eq E5) was calculated. Iglesia et al.[26,62] reported a similar linear trend between conversion rate and D_{Co} on impregnated Co supported on Al_2O_3, SiO_2, TiO_2, SiO_2-modified TiO_2, and $MgCr_2O_4$. The TOF values of these materials ranged between 0.016 and 0.030 s^{-1}, which were similar but slightly lower compared to the values obtained in the present work. The small deviation is probably due to the difference in the FT test condition.

The C_{5+} selectivities here are consistently above 87% for all the materials studied. All the samples tested here have structural parameter (χ) values in the range of 0.55−2.68 × 10^{19} m^{-1} (Table 3), for which the model by Iglesia et al.[26] would predict C_{5+} selectivity ∼90%. Interestingly, despite differences within each synthesis method, the effects of Ru-doping on the product selectivity of both impregnated and mechanically mixed materials were very similar. In the absence of Ru, both samples have carbon selectivities, S_{C2-C4} ≈ 11% and S_{C5+} ≈ 88%. The addition of 0.4% Ru slightly enhanced the S_{C5+} > 93%. It was suggested that readsorption of α-olefins on Co−Ru catalysts was responsible for the higher chain propagation rate.[26]

3.6. General Discussion. The present study shows that FSP is an alternative and uncompromising route (in terms of activity and selectivity) for preparing cobalt nanocomposites with good dispersion of cobalt and high surface area, here applied to FT synthesis. The characterization of the as-prepared materials shows that cobalt is well-dispersed in the ZrO_2 matrix. The high dispersion and incorporation of cobalt, however, resulted in a more difficult reduction step. The addition of Ru promoter in small concentrations drastically enhanced the cobalt reducibility and gave higher dispersions, which consequently led to materials with high FT activities.

The promotional effect of Ru (with respect to undoped Co-ZrO_2) is more pronounced for FSP composites than for standard impregnated materials. Further research will be directed to investigate other promoters for FSP-prepared composites. In fact, the one-step FSP technique can be conveniently extended to incorporate promoters, such as Pt,[29,63–65] Pd,[66,67] Rh[68] and even Re. This is particularly attractive as the technique offers the flexibility in designing different complex materials in a single step at short time scales (residence time of milliseconds) with reproducible properties. Even multicomponent noble metal promoters and alloying of these deposits are possible by FSP.[69]

While the unique structure of FSP-made cobalt−zirconia is demonstrated here for Fischer−Tropsch synthesis, the material itself is certainly not only restricted to catalytic applications.[1–13] The composite nanomaterial (both in as-prepared and reduced form) appears interesting for a number of applications such as solid state ionics (for solid oxide fuel cells)[70,71] and luminescence[72] and magnetic materials.[73]

4. Conclusions

A series of novel composite nanoparticles with highly dispersed Co_3O_4 (20 wt % Co) within the ZrO_2 matrix were made by one-step Flame Spray Pyrolysis. The high dispersion

(62) Iglesia, E. *Appl. Catal., A* **1997**, *161*, 59.
(63) Strobel, R.; Stark, W. J.; Mädler, L.; Pratsinis, S. E.; Baiker, A. *J. Catal.* **2003**, *213*, 296.
(64) Stark, W. J.; Grunwaldt, J. D.; Maciejewski, M.; Pratsinis, S. E.; Baiker, A. *Chem. Mater.* **2005**, *17*, 3352.
(65) Teoh, W. Y.; Mädler, L.; Amal, R. *J. Catal.* **2007**, *251*, 271.
(66) Strobel, W. J.; Krumeich, F.; Stark, W. J.; Pratsinis, S. E.; Baiker, A. *J. Catal.* **2004**, *222*, 307.
(67) Grunwaldt, J.-D.; Kimmerle, B.; Hannemann, S.; Baiker, A.; Boye, P.; Schroer, C. G. *J. Mater. Chem.* **2007**, *17*, 2603.
(68) van Vegten, N.; Ferri, D.; Maciejewski, M.; Krumeich, F.; Baiker, A. *J. Catal.* **2007**, *249*, 267.
(69) Hannemann, S.; Grunwaldt, J.-D.; Lienemann, P.; Günther, D.; Krumeich, F.; Pratsinis, S. E.; Baiker, A. *Appl. Catal., A* **2007**, *316*, 226.
(70) Dhalenne, G.; d'Yvoire, F.; Berthet, P.; Revclevschi, A. *Solid State Ionics* **1993**, *63−65*, 396.
(71) Lafleurielle, M.; Millot, F.; Dhalenne, G.; Revcolevschi, A. *Solid State Ionics* **1996**, *89*, 139.
(72) Rodríguez, R.; Jiménez-Sandoval, S.; Estevez, M.; Pacheco, S.; Vargas, S. *J. Sol−Gel Sci. Technol.* **2007**, *44*, 97.
(73) Liu, Z.; Shindo, D.; Ohnuma, S.; Fujimori, H. *J. Magn. Magn. Mater.* **2003**, *262*, 308.

coupled with strong cobalt−zirconia interactions was reflected in the high reduction temperature of the materials. Nevertheless, doping of Ru (0.04 and 0.4%) as a promoter significantly decreased the temperature required for the two-step reduction of Co_3O_4 to CoO and to metallic Co^0. More importantly, the well-dispersed Ru promoter within the composite particles increased the cobalt reducibility significantly, reducing even the cobalt embedded in the zirconia matrix. Because of the milder reducibility, doping with 0.4% Ru in FSP-made composites resulted in a better dispersion of the metallic cobalt as reflected by the nearly 4-fold enhancement in CO chemisorption.

The structural and physicochemical properties of the cobalt−zirconia composite materials were well-reflected in its catalytic performance. The Fischer−Tropsch synthesis activity, evaluated by CO conversion, improved proportionally with the increase in metallic Co active sites (higher dispersion). The FT activity of FSP-made 0.4% Ru-doped cobalt−zirconia, which had the highest metallic Co dispersion, matches the performance of benchmark impregnated catalyst. Furthermore, the cobalt active sites of flame-made composites exhibited similar turnover frequencies as both impregnated and mechanically mixed samples.

Acknowledgment. The authors gratefully acknowledge the technical supports of Dr. Yun Lei (UNSW) on TPR, chemisorption, and GC-MS analyses. The generosity of Prof. David L. Trimm and Dr. Dean Chambers (CSIRO Petroleum) in allowing the usage of FT reactors is much appreciated. The authors also thank Dr. Frank Krumeich (ETH Zürich) for the electron microscopy analyses and Björn Schimöller for assistance. L.M. thanks the Deutsche Forschungsgemeinschaft DFG (German Research Foundation, Forschungsstipendium MA3333/1-1) for support.

Supporting Information Available: Equations for calculating dispersion size, CO conversion rate, cobalt time yield, turnover frequencies, and structural parameters (PDF). This material is available free of charge via the Internet at http://pubs.acs.org.

CM8002657